Active Water Molecule Transport in Biological Tissue: Underpinnings of MRI Interpretation

Charles Springer

William Rooney, Xin Li, Wei Huang

OHSU

Oregon Health & Science University

Advanced Imaging Research Center

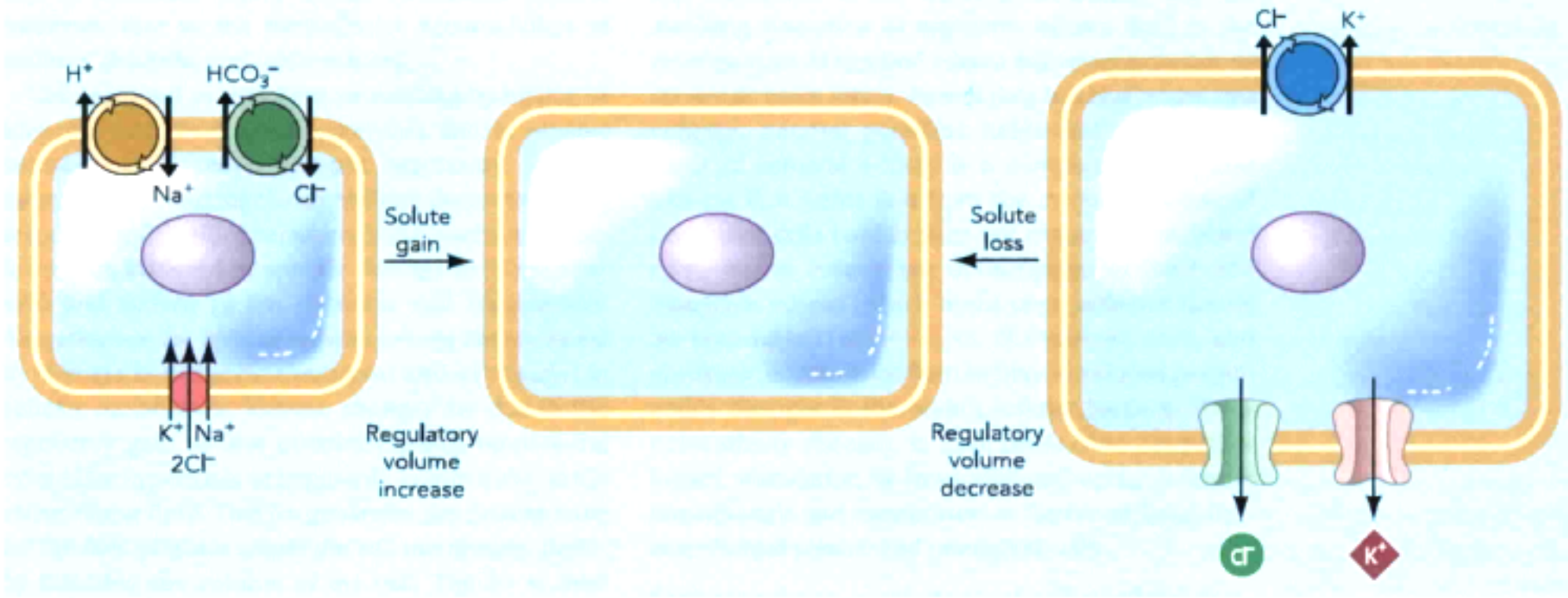

FIGURE 1. **Molecular mediators of cell volume regulation / edema**
The homeostatic counter-responses that maintain normal cell volume are mediated by changes in the activity of ion transporters and channels, which occur within seconds of the volume perturbation. Acute cell shrinkage is countered by regulatory volume increase, which triggers the activation of the bumetanide-sensitive NKCC1 cotransporter, resulting in the influx of sodium (with chloride and potassium) and water, thereby increasing cell volume. Other sodium influx pathways like the Na^+/H^+ exchanger NHE1, working in concert with the Cl^-/HCO_3^- exchanger, are also involved. Acute cell swelling is countered by regulatory volume decrease, which involves the cellular loss of chloride and potassium via the activation of the K-Cl cotransporters and swelling-activated potassium and chloride channels. Ischemia-triggered increases in NKCC1 and other ion carriers can cause cytotoxic edema or isosmotic cell swelling. Figure from Ref. 33 and used with permission.

Kahle, Simard, Staley, Nahed, Jones, Sun (2009)

$$k_{io} = 1/\tau_i = C(P_W/d)$$

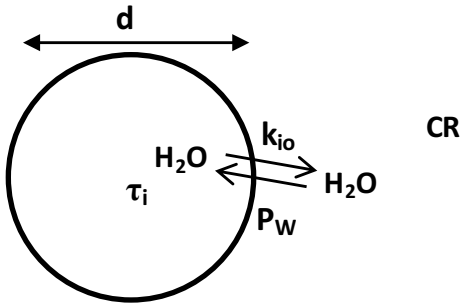

for spherical (cylindrical) cell: C = 6 (4)

for d = 20 μm: $1/\tau_i = 2000\ P_W$ [τ_i in s; P_W in cm/s]

for $P_W = 5 \times 10^{-4}$ cm/s: $1/\tau_i = 20$ (1/d) [d in μm]

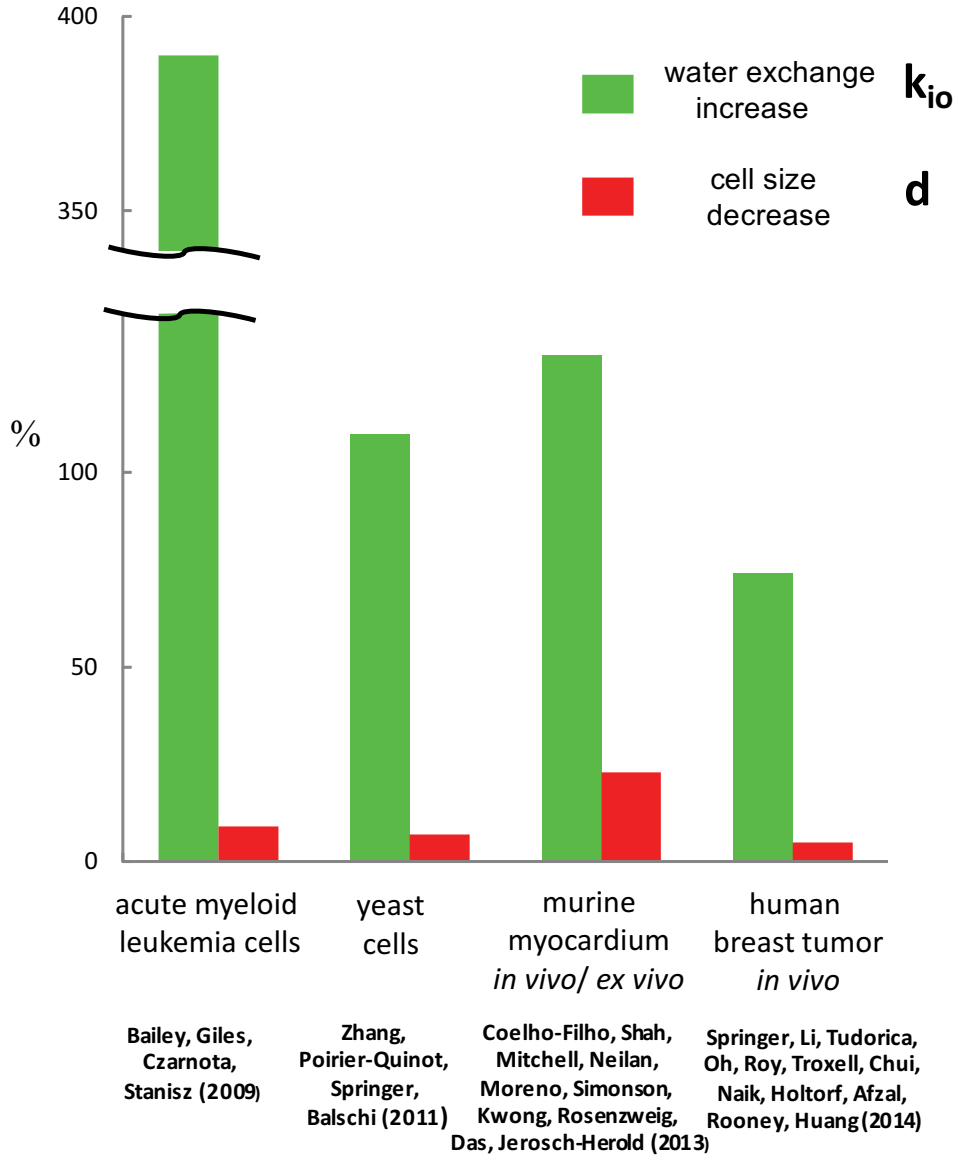

Springer, Li, Tudorica, Oh, Roy, Chui, Naik, Holtorf, Afzal, Rooney, Huang (2014)

P-type ATPases

Na^+,K^+-ATPase [NKA]

H^+-ATPase [Pma1]

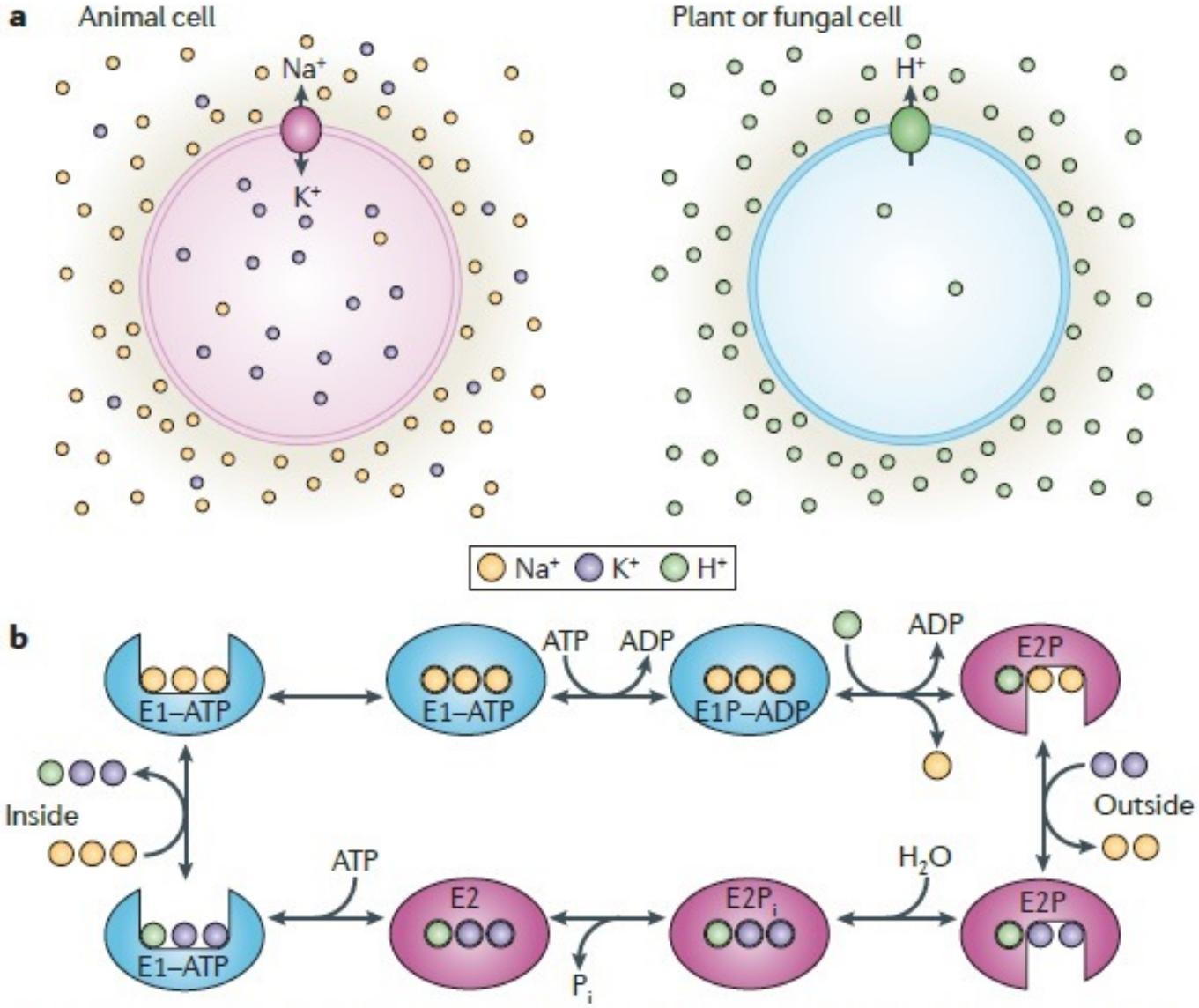

Figure 1 | **P-type ATPases energize the plasma membrane**. The plasma membrane of all eukaryotic cells is energized by a P-type ATPase, which exports cations and cause a separation of charge across the membrane. The energy of stored electrochemical gradients is used by numerous other transport systems; for example, to drive nutrient uptake and generate the basis for action potentials. **a** | In animal cells the plasma membrane is energized by the Na^+,K^+-ATPase, which exports three Na^+ and imports two K^+ for every ATP hydrolysed. In fungi and plants, the plasma membrane is energized by a H^+-ATPase, which exports one H^+ for every ATP hydrolysed, with no counter ion transported in the opposite direction. In this way, the pump reaction causes efflux from the cell of a net positive charge carried by H^+. **b** | The reaction cycle of a P-type ATPase, represented by the Na^+,K^+-ATPase. Binding of Na^+ to the E1–ATP state from inside the cell triggers phosphorylation, leading to the formation of the occluded [Na_2]E1P–ADP state (represented by a 'closed' form) and a subsequent transition to the E2P state. The E2P state has reduced affinity for Na^+, leading to exchange of three Na^+ for two K^+ from outside the cell and also a cytoplasmic proton at a vacant ion-binding site[105]. Closure of the E2P state leads to E2P dephosphorylation and formation of the occluded [K_2]E2 state. ATP binding leads to formation of the E1 state and consequent release of K^+ inside the cell and binding of Na^+.

Morth, Pedersen, Buch-Pedersen, Andersen, Vilsen, Palmgren, Nissen (2011)

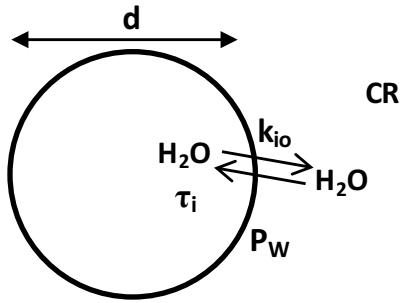

$$ATP_i + H_i^+ \xrightarrow{Pma1} ADP_i + P_i + H_o^+$$

$$ATP_i + 2K_o^+ + 3Na_i^+ \xrightarrow{NKA} ADP_i + P_i + 2K_i^+ + 3Na_o^+$$

Table 1. τ_i^{-1} (k_{io}) Reflects Turnover of Driving Membrane P-Type ATPase Ion Pump

P-Type ATPase Ion Pump	yeast	cardiomyocyte	erythrocyte
gene dosage	↑↑[24]		
substrate			
ATP_i	↑↑[24]		↑↑[75]
K_o^+		↑↑[26]	
specific inhibitor			
ebselen	↑↓[24]		
ouabain		↑↓[26]	

↑↑ positively related; ↑↓ inversely related

[24]measured; Zhang, Poirier-Quinot, Springer, Balschi (2011)

[26]measured; Zhang, Balschi (2013)

[75]inferred; Kuchel, Benga (2005)

Springer, Li, Tudorica, Oh, Roy, Chui, Naik, Holtorf, Afzal, Rooney, Huang (2014)

The Na^+,K^+-ATPase System

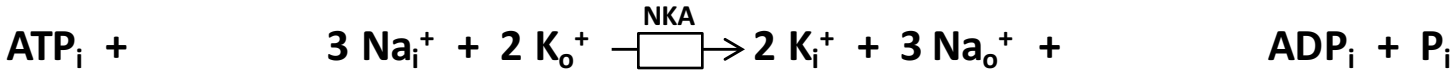

The Na^+,K^+-ATPase System

The Na^+,K^+-ATPase System

$ADP_i + PCr_i \xrightleftharpoons{CrK} ATP_i +$

$3\ Na_i^+ + 2\ K_o^+ \xrightarrow{NKA} 2\ K_i^+ + 3\ Na_o^+ +$

$ADP_i + P_i$

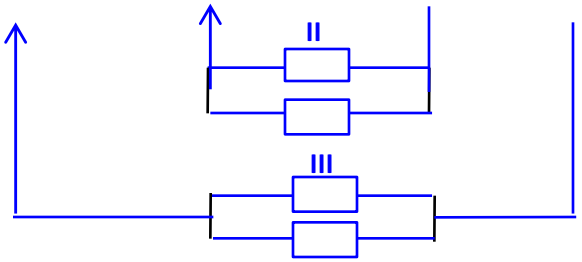

The Na^+,K^+-ATPase System

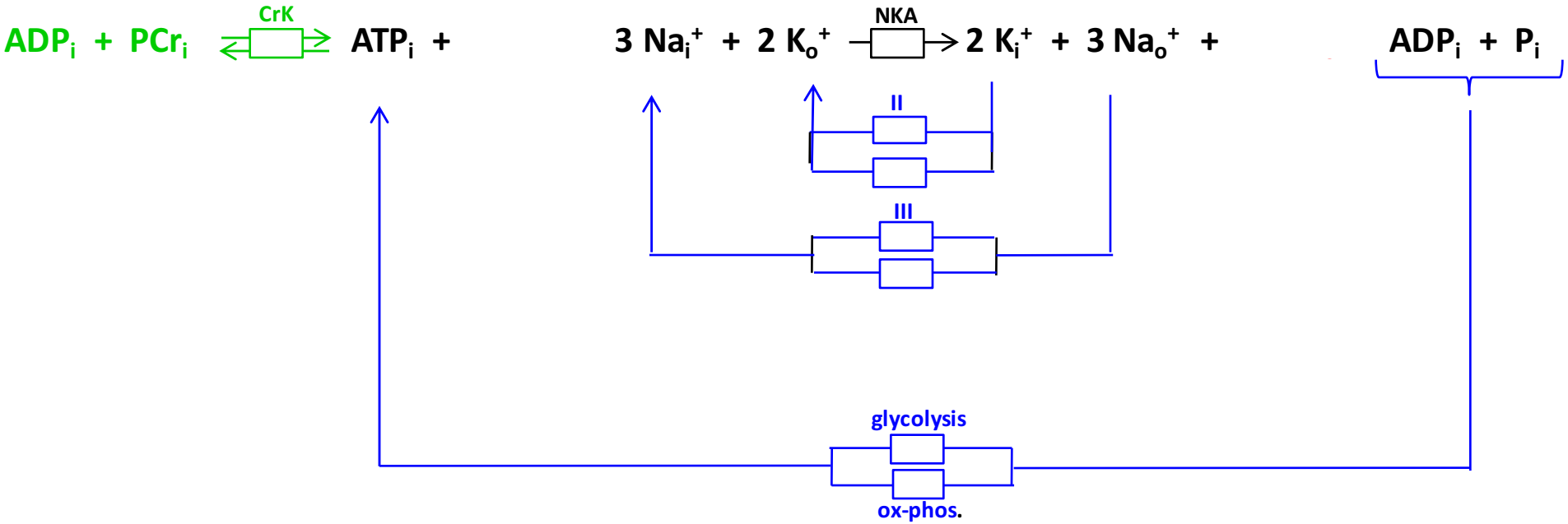

The Na^+,K^+-ATPase System

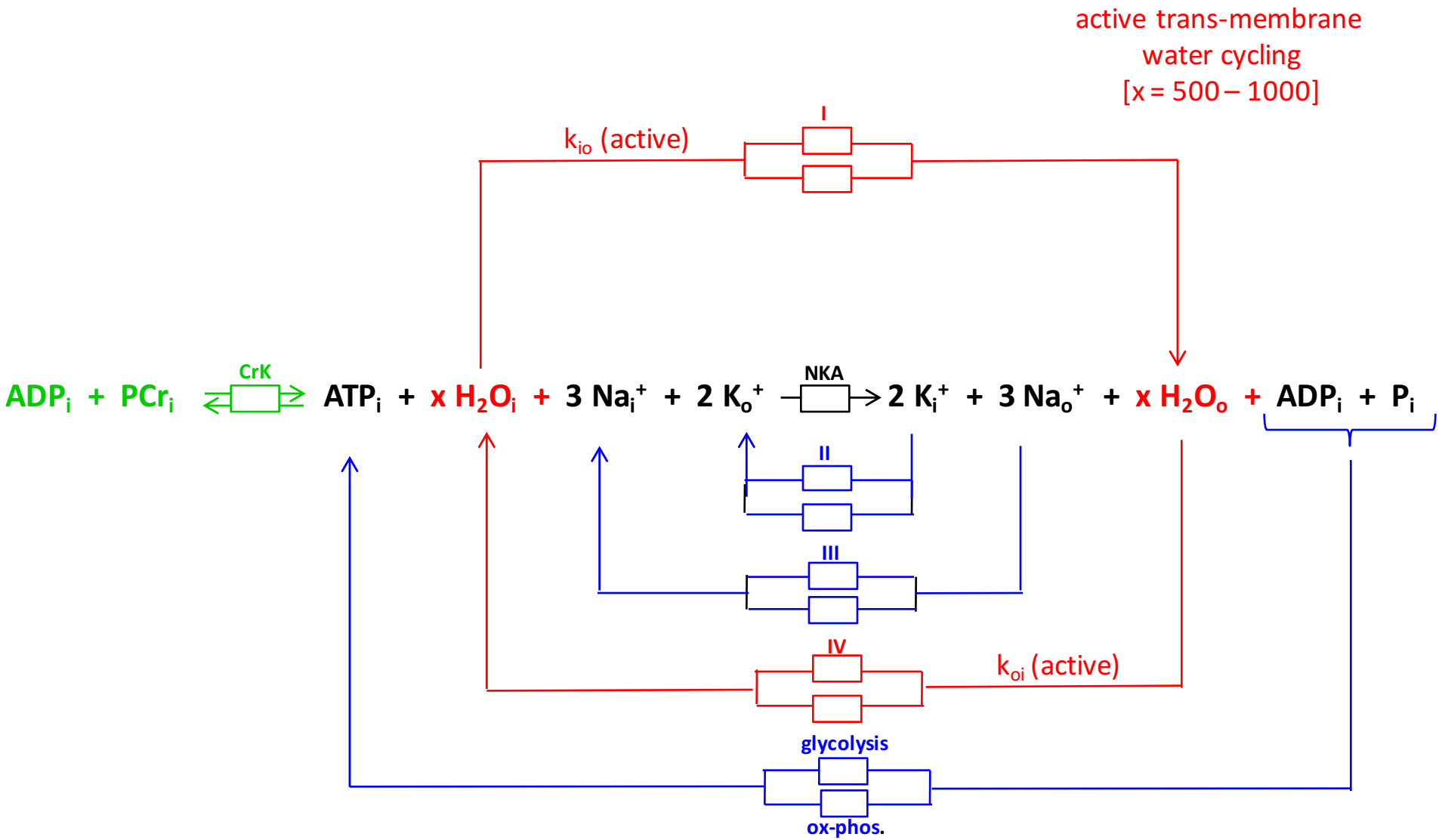

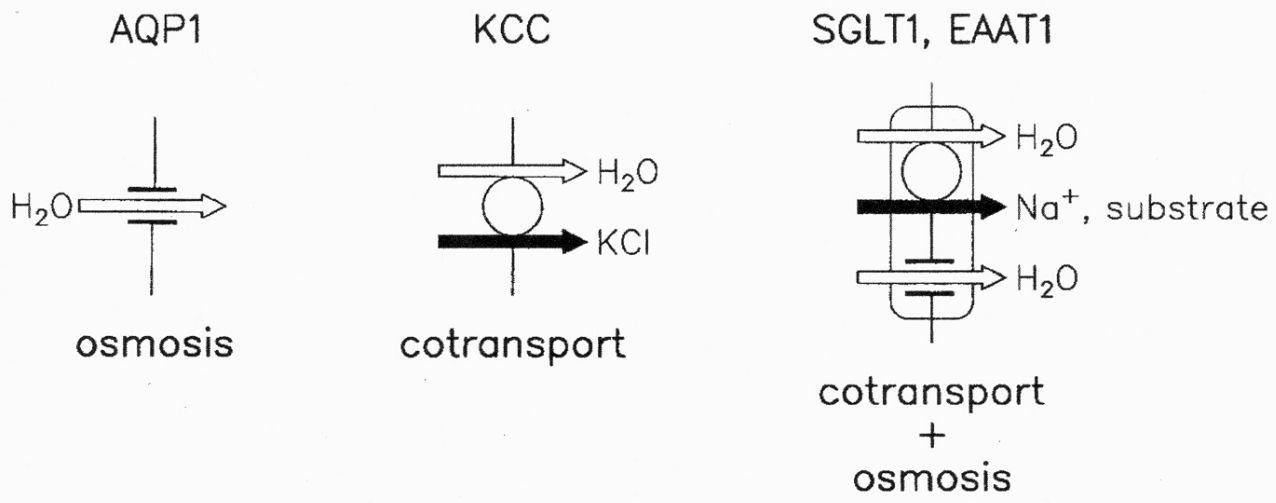

Fig. 1 Molecular mechanism of water transport across cell membranes. Water crosses membranes by diffusion in the lipid bilayer, by osmosis in channels and by cotransport in cotransporters and uniporters. Diffusion and osmosis are driven by the water chemical potential difference. The cotransporters and the uniporters function as molecular water pumps in which free energy contained in the substrate gradient can be transferred to the transport of water; i.e., a downhill transport of substrate can energize an uphill transport of water. Some cotransporters, such as the KCC, employ only cotransport; others, such as the SGLT1 and the EAAT1, employ both cotransport and osmosis

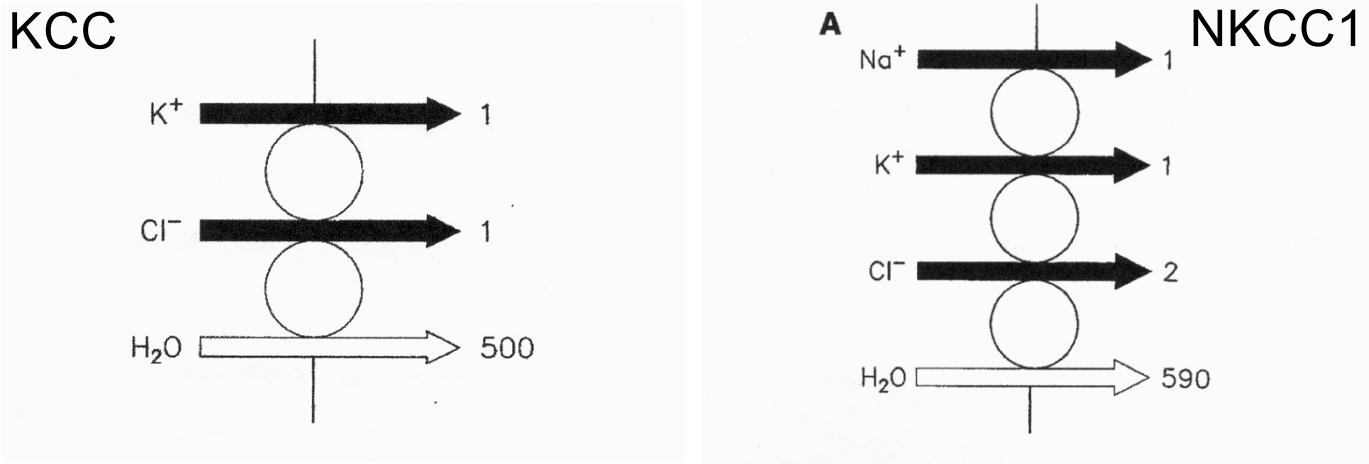

T. Zeuthen (2010)

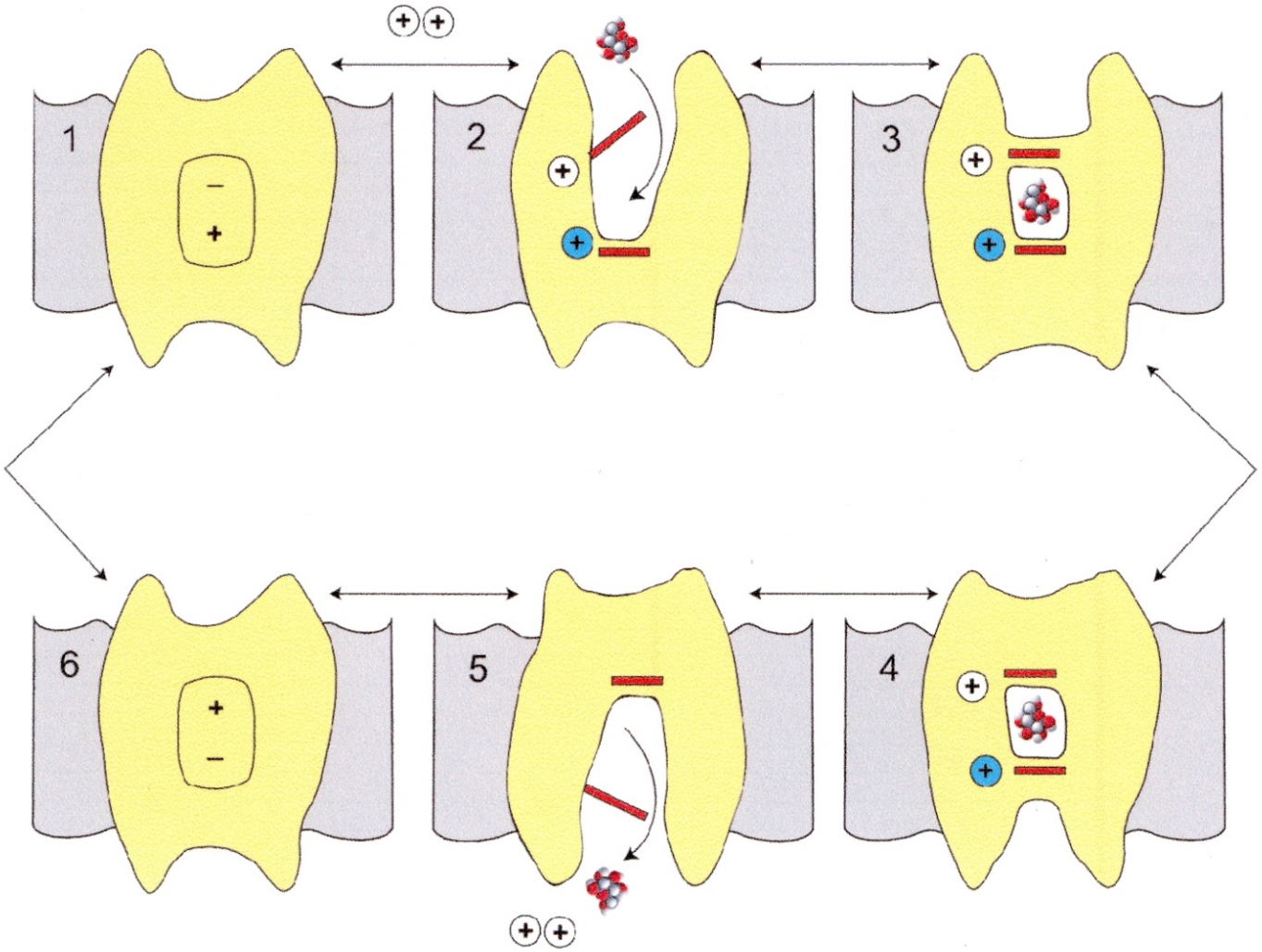

FIG. 31. A 6-state model of SGLTs to integrate the kinetic and structural data. Na^+ binds first to the outside to open the outside gate (C2) permitting outside sugar to bind and be trapped in the binding site (C3). This is followed by a conformational change from an outward occluded (C3) to an inward occluded (C4) state. Upon opening the inward gate (C5), the Na^+ and sugar are released into the cell interior. There is a paucity of experiments adressing the order of the ligand dissociation at the cytosolic surface. The transport cycle is completed by the change in conformation from the inward facing ligand-free (C6) to the outward facing ligand free (C1) states. Structures corresponding to C2 and C3 have been obtained for Mhp1, C3 for LeuT, and C4 for vSGLT.

Wright, Loo, Hirayama (2011)

Active Trans-Plasma Membrane Water Cycling

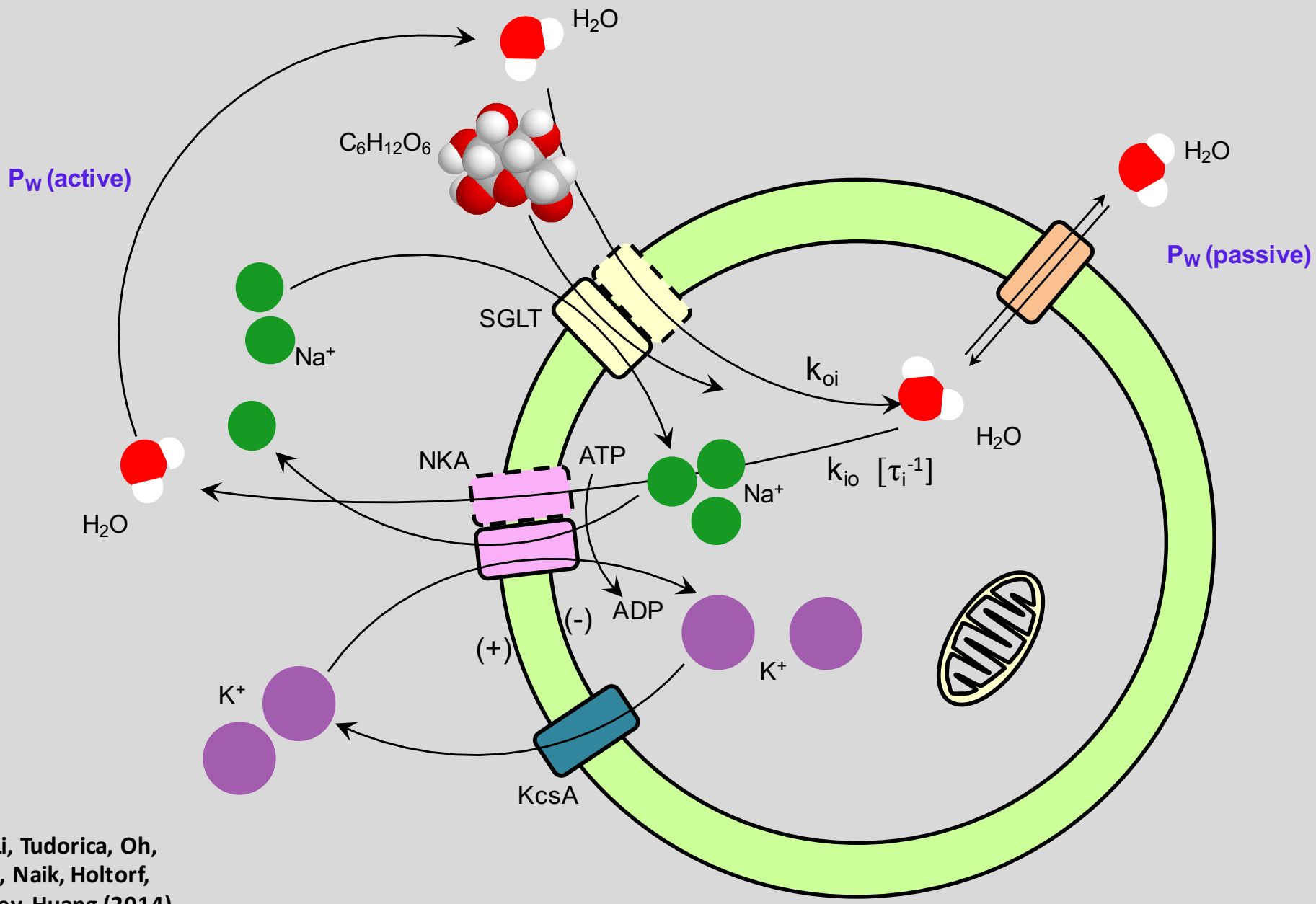

Springer, Li, Tudorica, Oh, Roy, Chui, Naik, Holtorf, Afzal, Rooney, Huang (2014)

general glucose metabolism

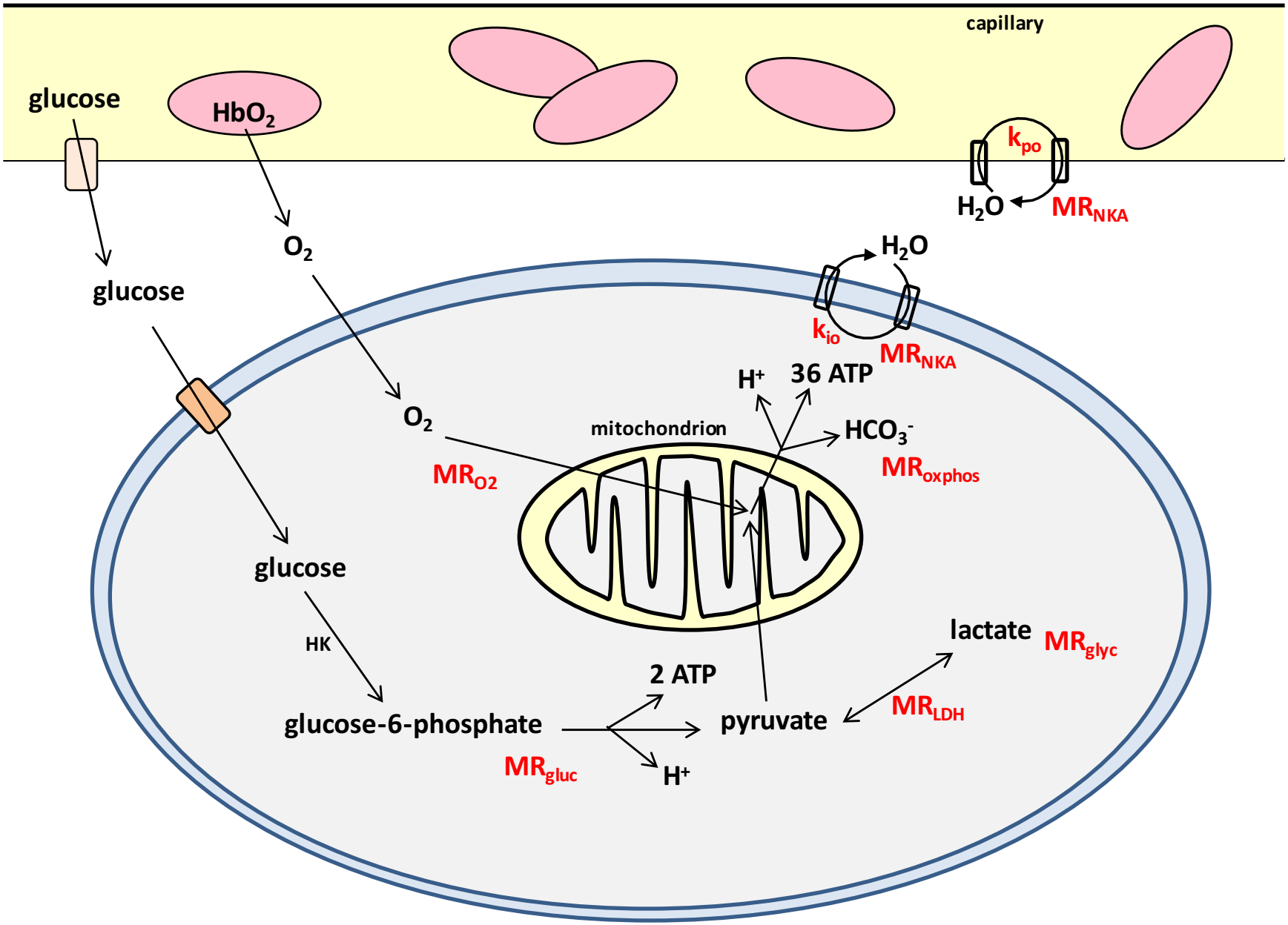

Springer

[Dynamic-Contrast-Enhanced] DCE-MRI

3T / malignant prostate

no endorectal RF coil

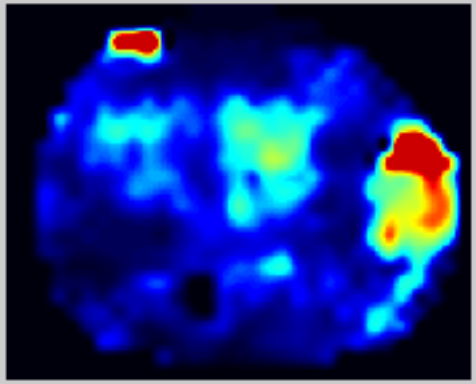

66 yo

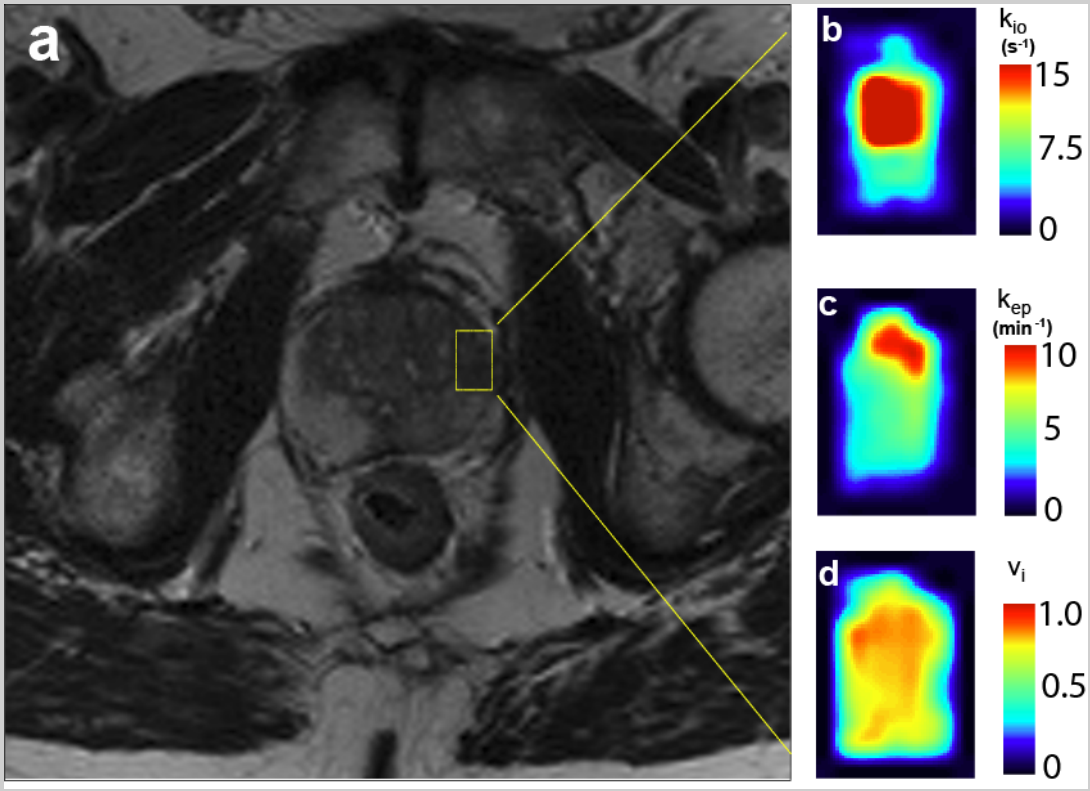

k_{io} [$\equiv \tau_i^{-1}$] (s^{-1})

adenocarcinoma

$\langle k_{io} \rangle_{ROI}$ (s^{-1}) *in vivo*

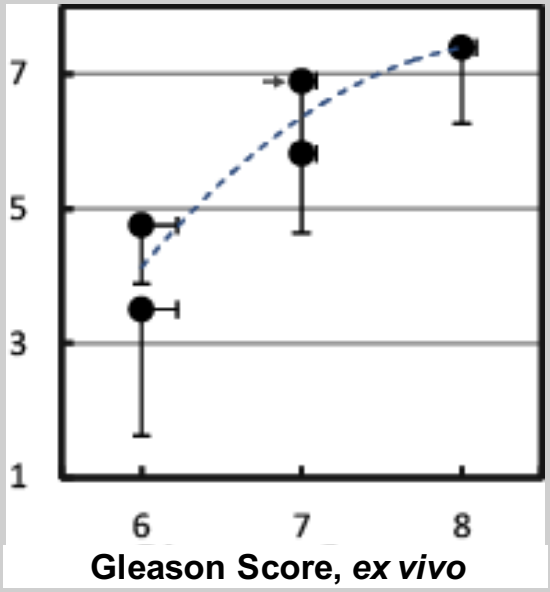

5 subjects

Li, Yu, Moloney, Chen, Huang, Woods, Coakley, Rooney, Garzotto, Springer

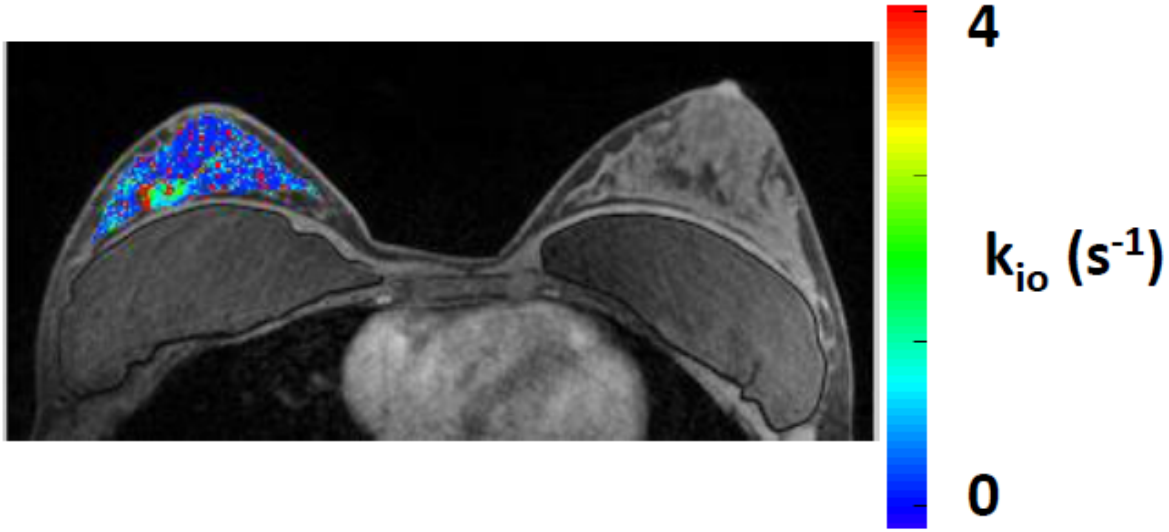

Tudorica, Oh, Chui, Roy, Troxell, Naik, Kemmer, Chen, Holtorf, Afzal, Springer, Li, Huang

3T
human breast tumor [No. 13]
(grade 2 IDC; HER2+; BRCA1/BRCA2-; ER+; PR-)
paclitaxel/cyclophosphamide + adriamycin

V1–[NACT]-V2–[NACT]–[NACT]-V3–[NACT]–[NACT]–[NACT]-V4-p

29 human primary breast tumors

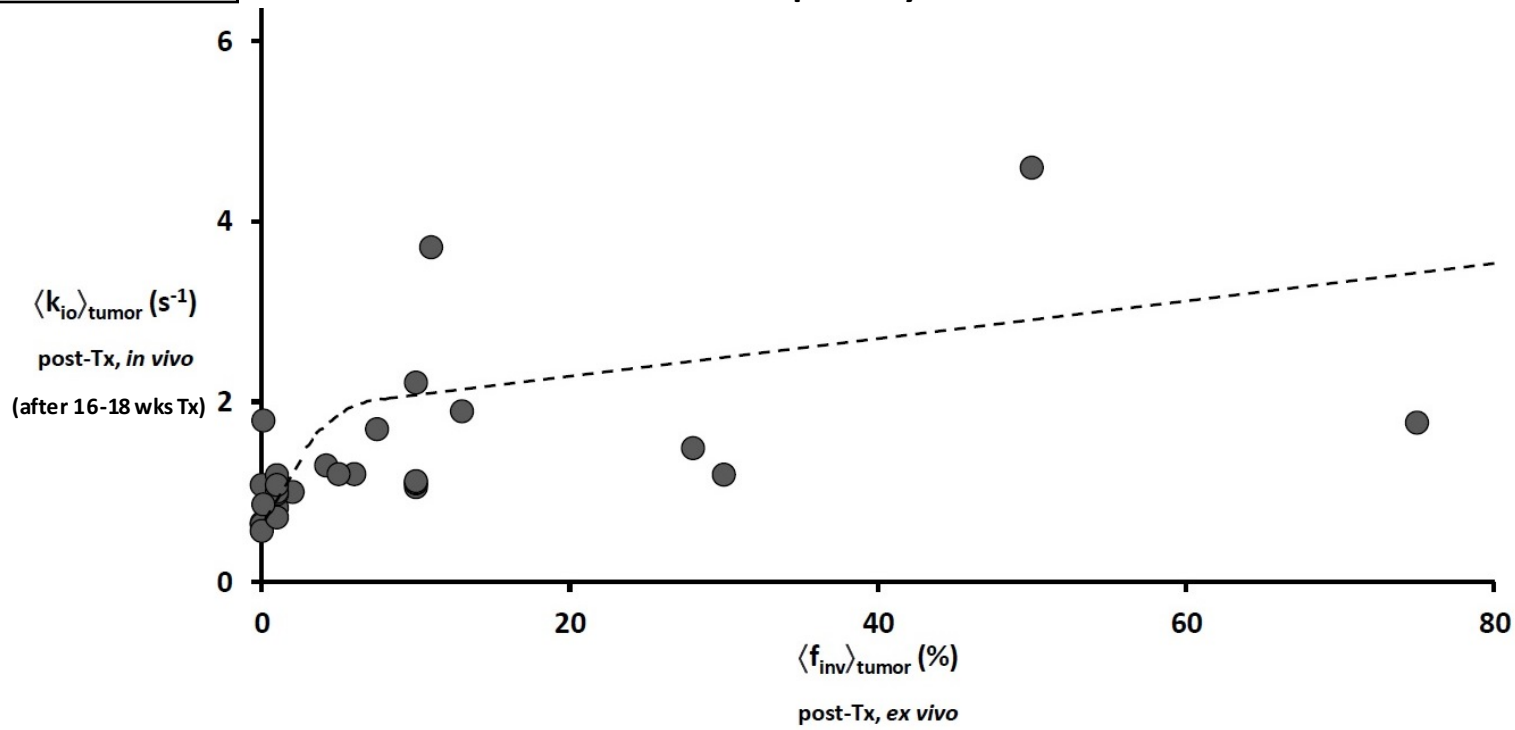

Accardi (2015)

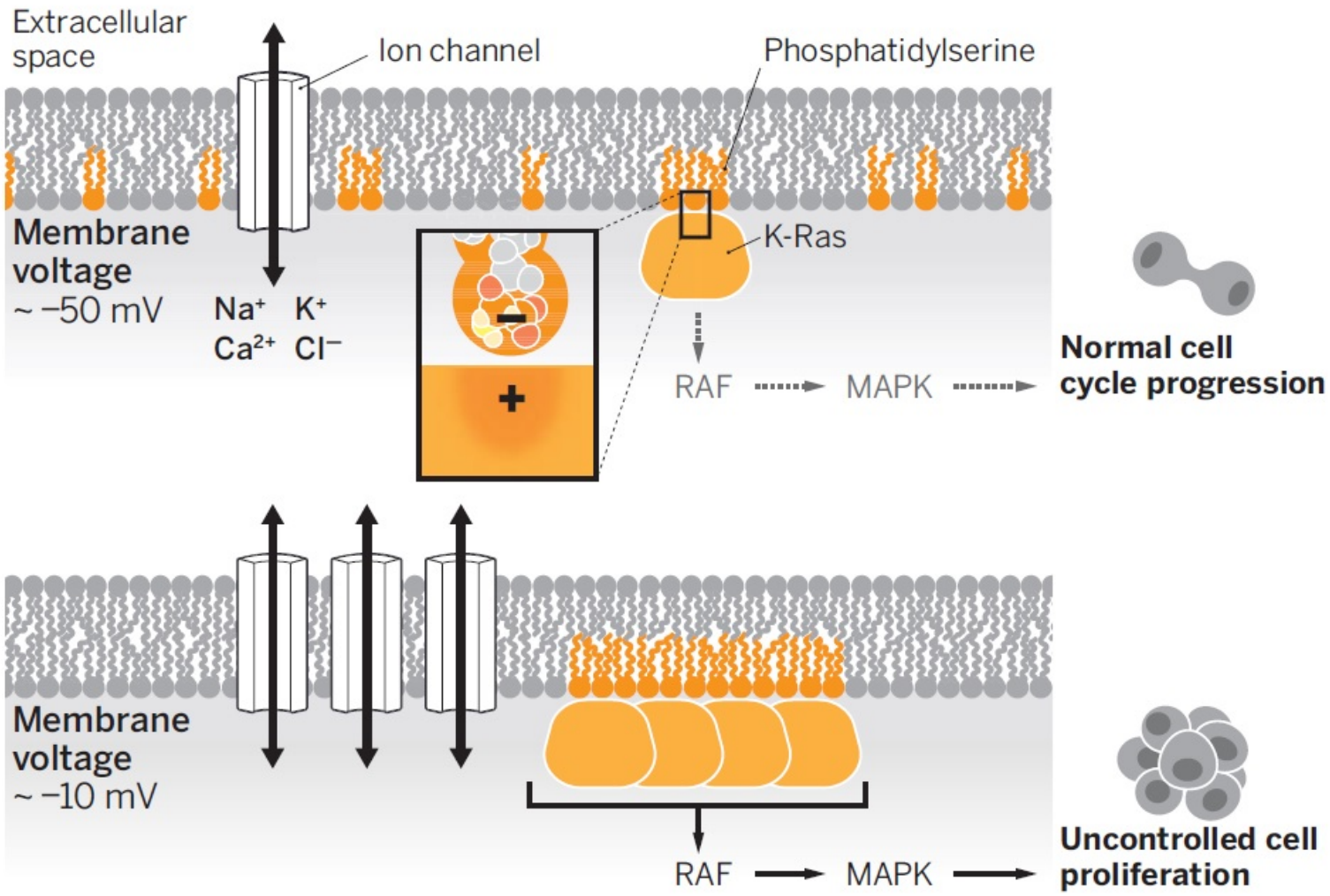

Potential and proliferation. In a normal, nonproliferating cell, the resting membrane potential ($V_m \approx -50$ mV) is set by ion channel activity. Phosphatidylserine lipids are in small clusters that localize with K-Ras, which leads to low activation of the RAF-MAPK pathway. Channel overexpression depolarizes the cell ($V_m \approx -10$ mV), increasing the clustering of phosphatidylserine and K-Ras. This promotes RAF-MAPK signaling uncontrolled cell proliferation.

Zhou, Wong, Cho, van der Hoeven, Liang, Thakur, Luo, Babic, Zinsmaier, Zhu, Hu, Venkatachalam, Hancock (2015)

The Na^+,K^+-ATPase System

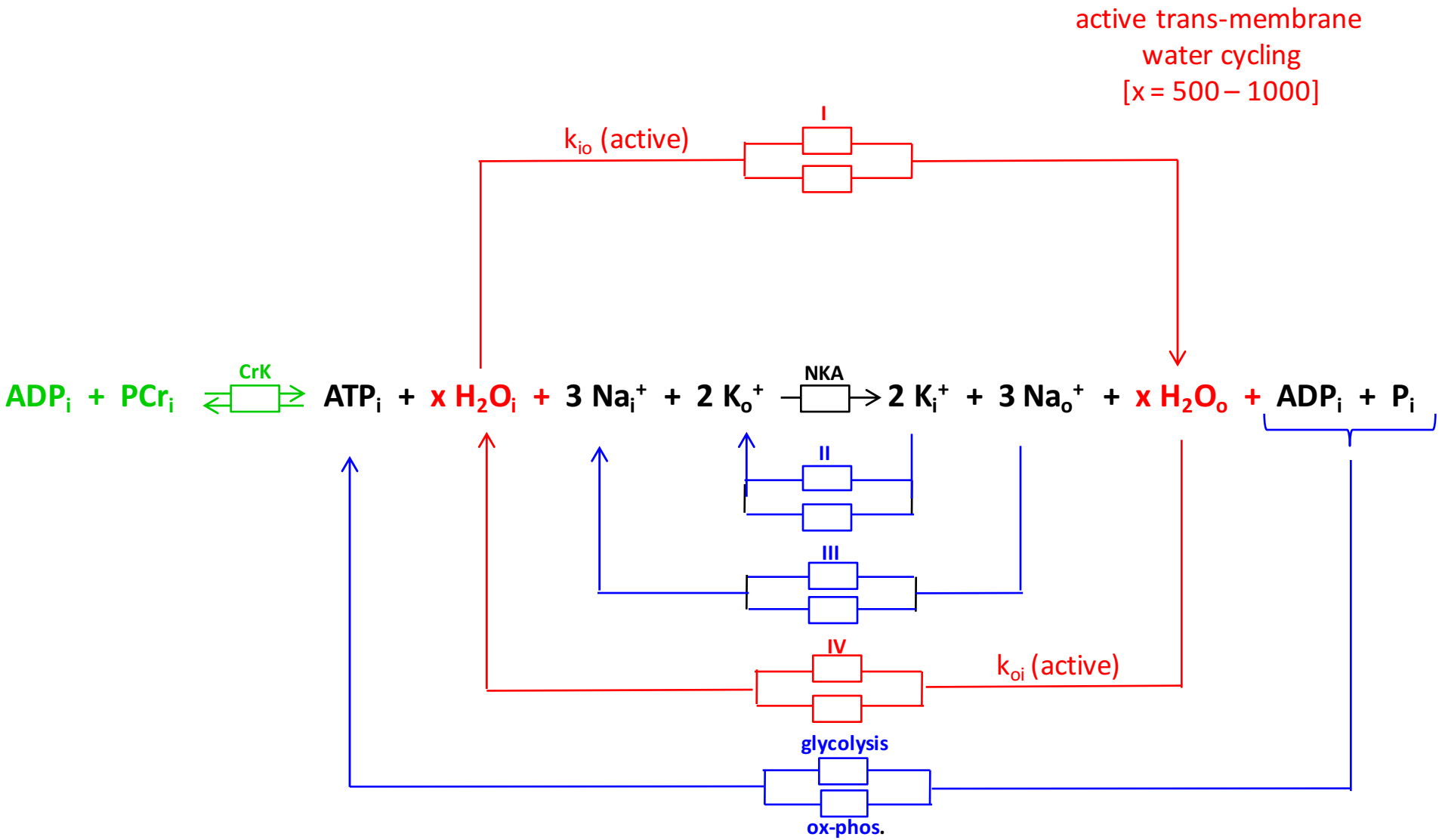

squamous cell carcinoma of the head and neck 1.5T

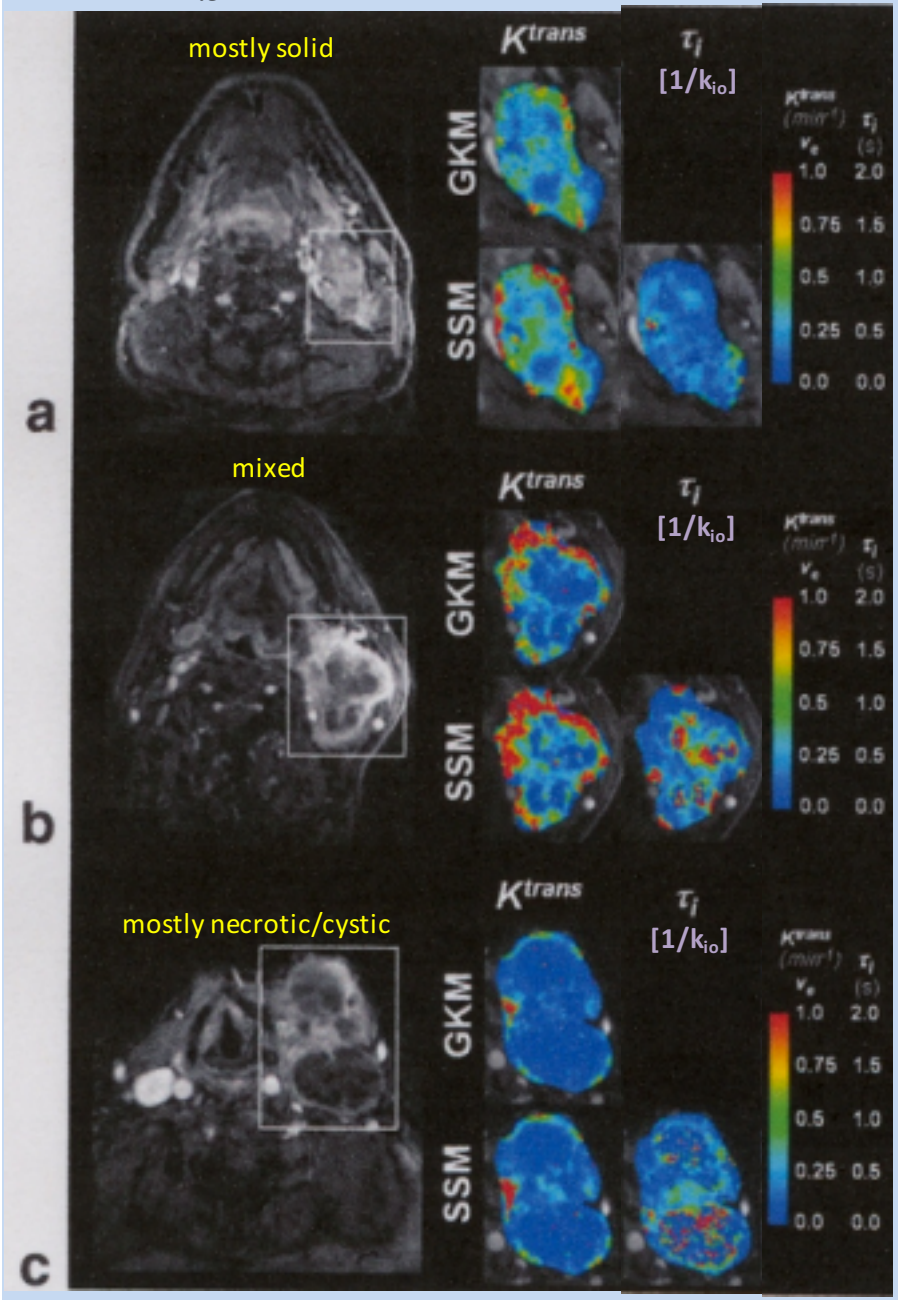

Kim, Quon, Loevner, Rosen, Dougherty, Kilger, Glickson, Poptani (2007)

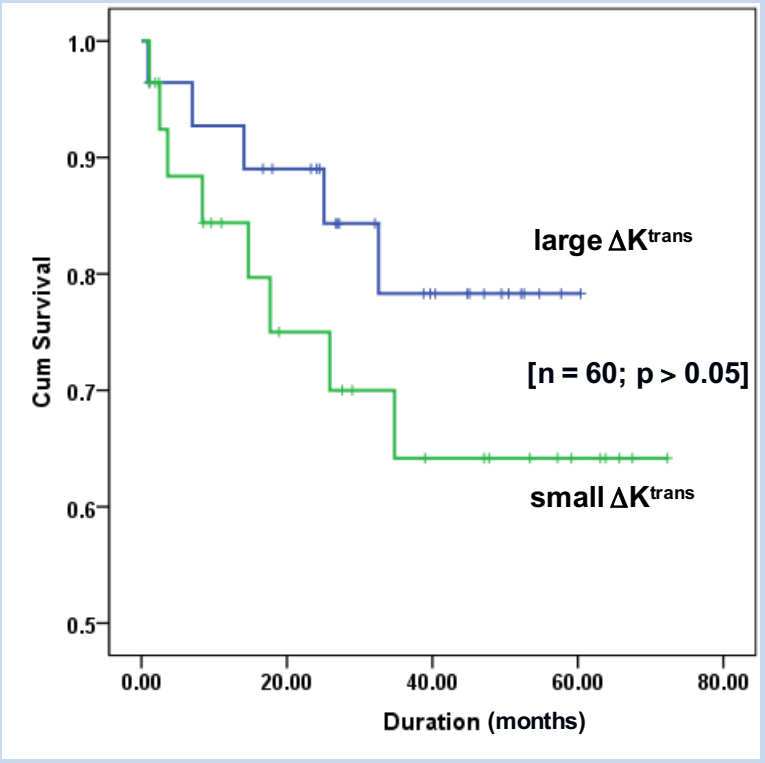

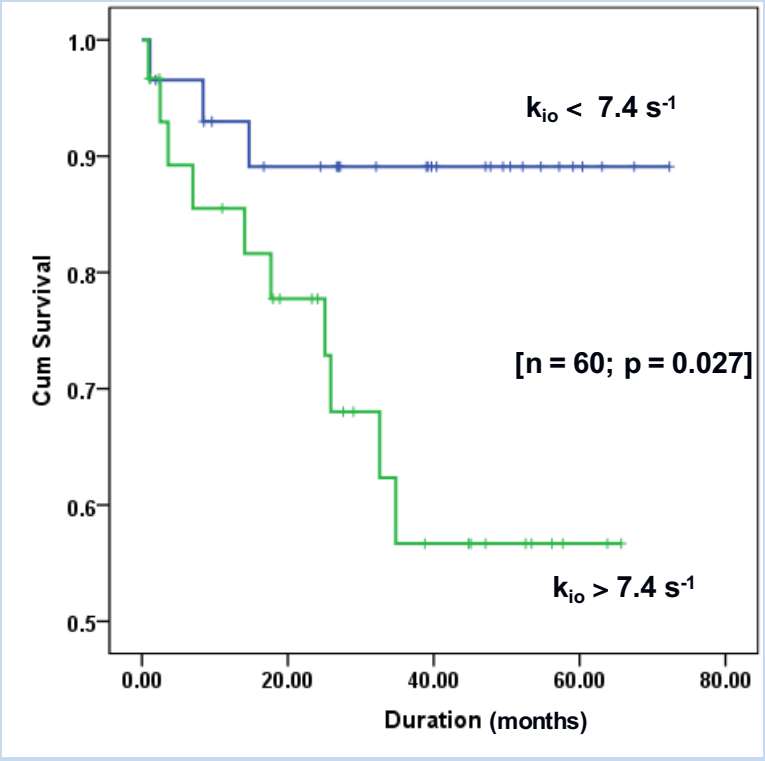

Poptani

3T

human breast tumor [No. 4, pCR]

(grade 2 IDC; HER2+; BRCA1/BRCA2-; ER+; PR+)

trastuzumab/paclitaxel

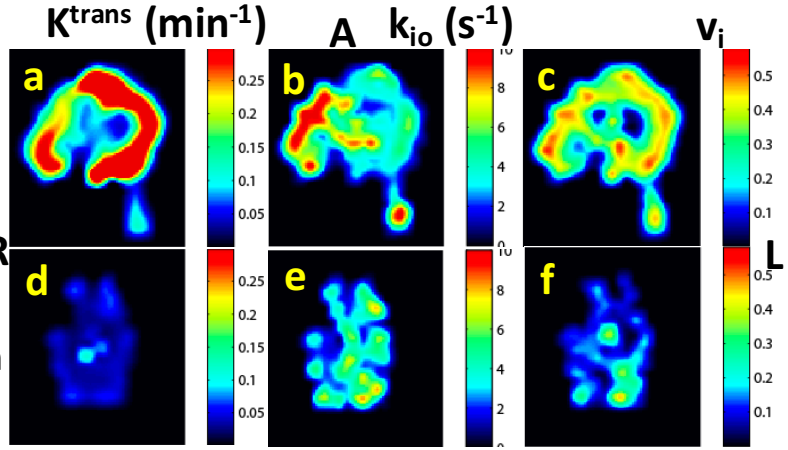

Figure 1.

V1–[NACT]-V2–[NACT]–[NACT]-V3–[NACT]–[NACT]–[NACT]-V4-p

29 human primary breast tumors

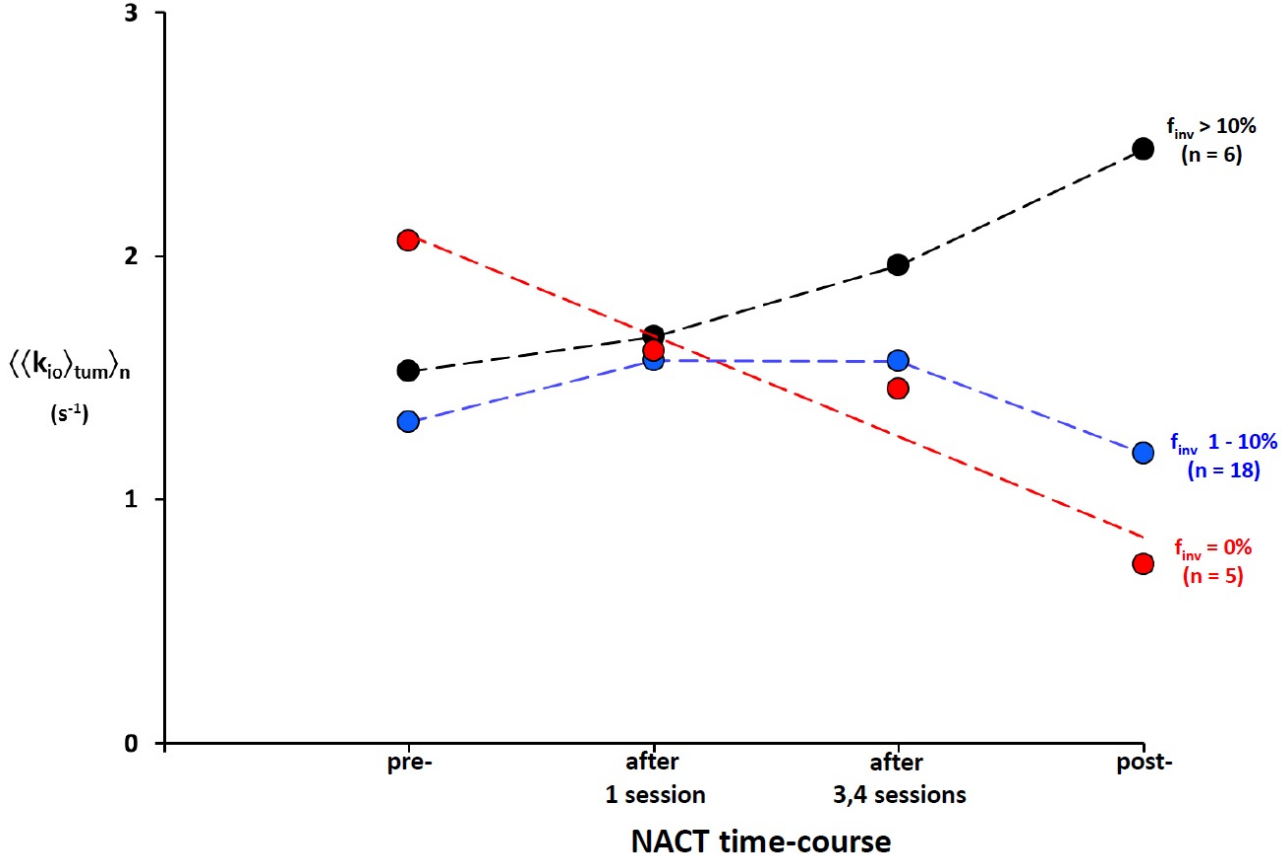

Tudorica, Oh, Chui, Roy, Troxell, Naik, Kemmer, Chen, Holtorf, Afzal, Springer, Li, Huang

human heart
[repaired Tetralogy of Fallot]
1.5T / {wash-out shutter-speed method}

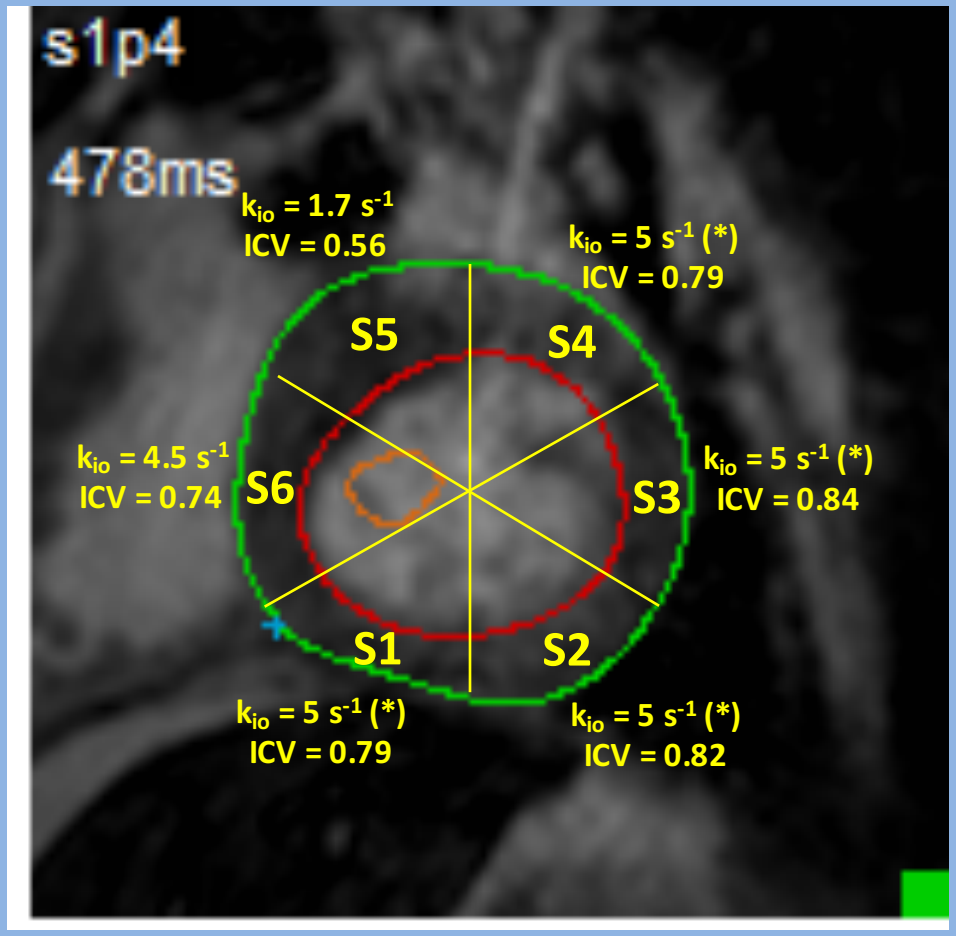

*set at ⟨normal value⟩

Rooney, Broberg, Springer (2015)

Myocardial Na^+,K^+-ATPase Turnover					
method	**myocardium**	**ECV**	**ICV [= ρ•V]**	**k_{io} (s^{-1})**	**reference**
steady-state shutter-speed	*ex vivo* rat (perfused/beating) control			5.6	a
	(no flow) ischemia			3.7	
	change			36%↓	
titration shutter-speed	*in vivo / ex vivo* mouse control [n = 13]	0.25	0.75	5.3	b
	chronic hypertension [n = 17]	0.42	0.58	2.3	
	change		23%↓	57%↓	
wash-out shutter-speed	*in vivo* human control [n = 12]	0.31	0.69		c
	chronic hypertension [n = 8]	0.45	0.55		
	change		20%↓		
wash-out shutter-speed	*in vivo* human control [n = 6]	0.33	0.67	5.0	d
wash-out shutter-speed	*in vivo* human control [n = 20]	0.31	0.69	10.0	e
	chronic infarct [n = 20]	0.61	0.39	2.5	
	change		43%↓	75%↓	

a. Poirer-Quinot, He, Springer, Balschi (2006).

b. Coelho-Filho, Shah, Mitchell, Neilan, Moreno, Simonson, Kwong, Rosenzweig, Das, Jerosch-Herold (2013).

c. Coelho-Filho, Mongeon, Mitchell, Moreno, Nadruz, Kwong, Jerosch-Herold (2013).

d. Springer, Broberg, Rooney (2014).

e. Goldfarb, Zhao (2014).

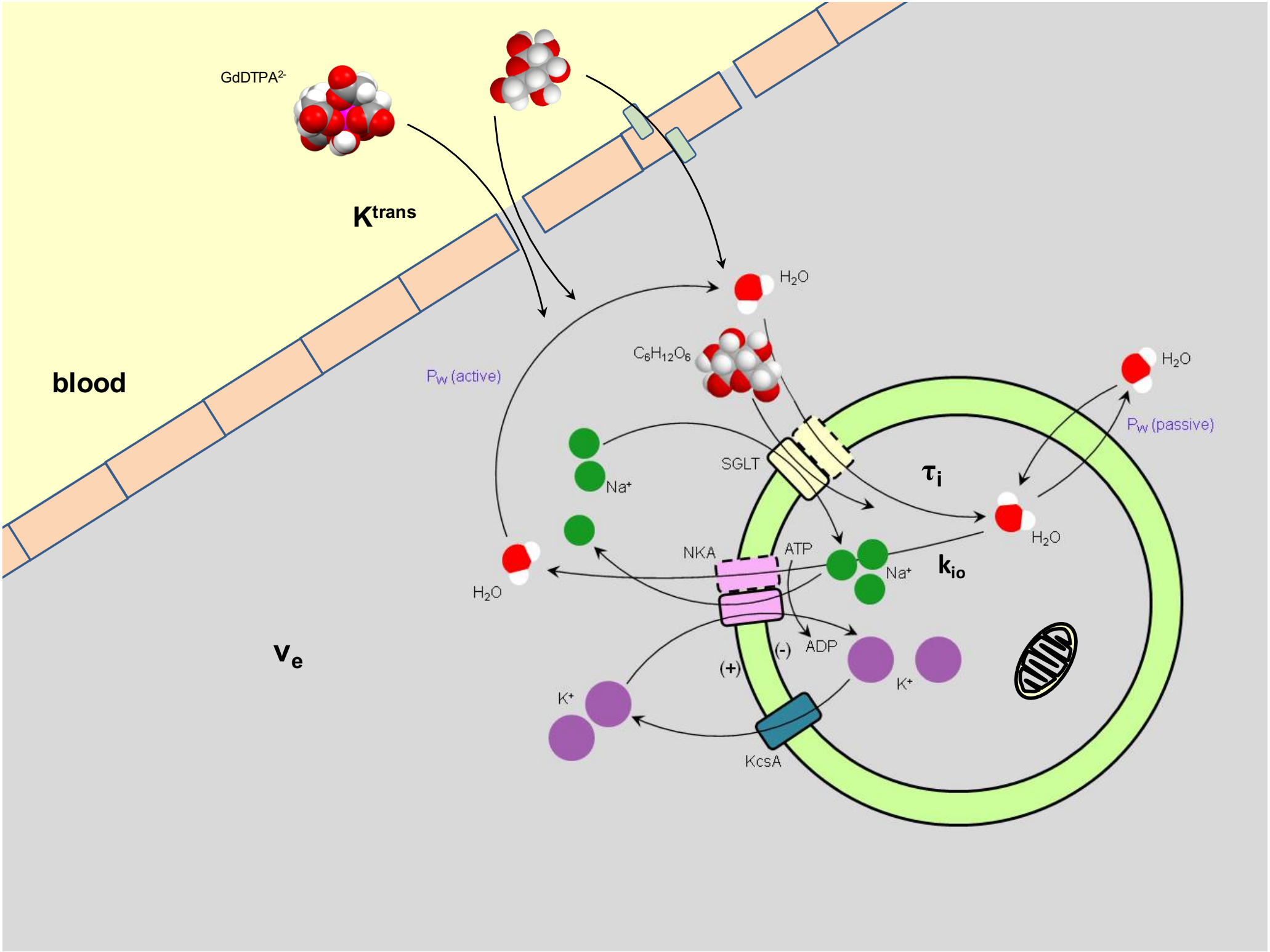
GdDTPA2-
Ktrans
blood
ve
H2O
C6H12O6
Pw (active)
Pw (passive)
SGLT
Na+
τi
NKA
ATP
kio
ADP
(-)
(+)
K+
KcsA

William D. Rooney

Brain Blood Vessel in Cross Section

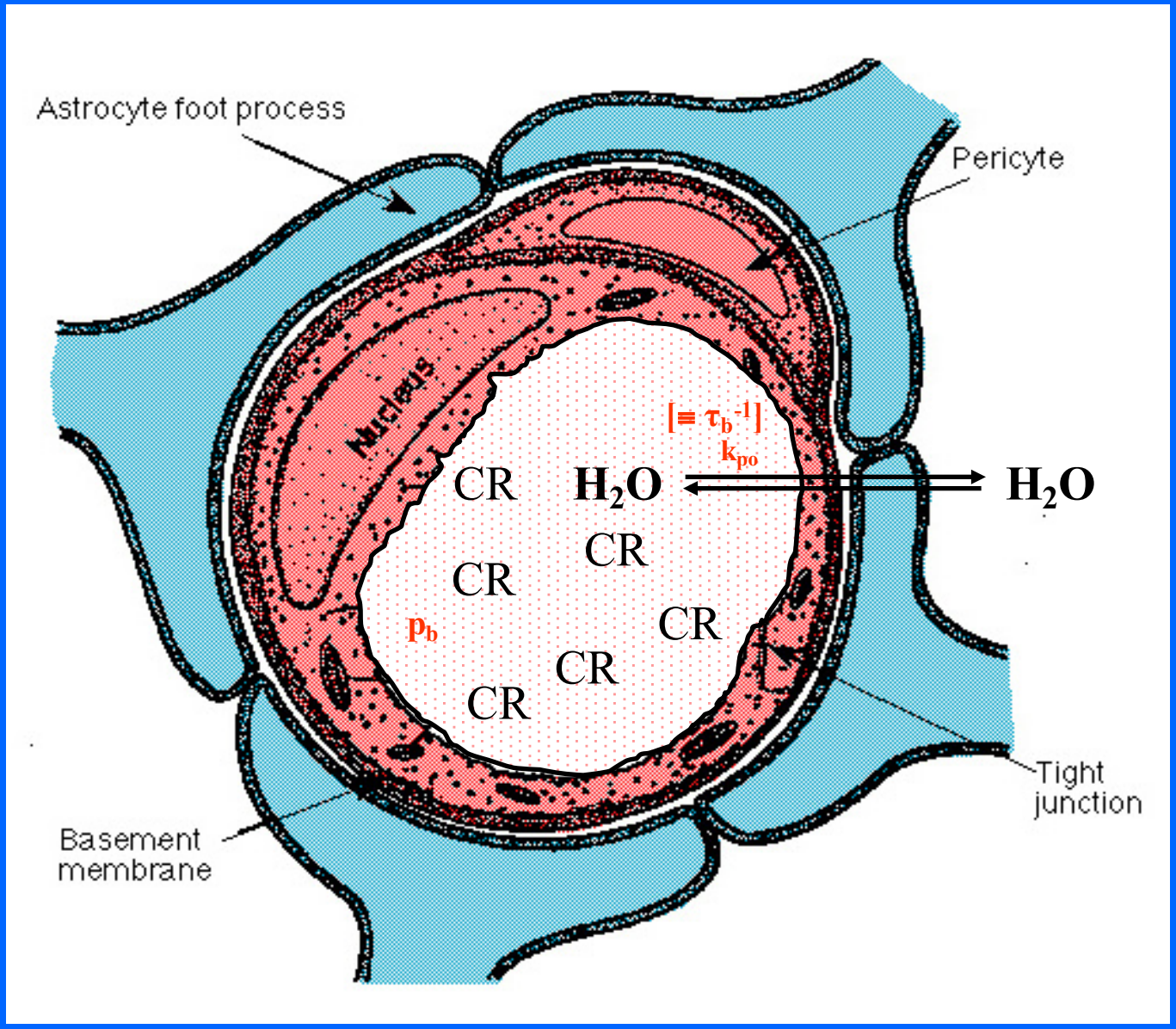

Trans-Capillary Water Exchange Modeling

Three variables:

1. $1/T_{1e}$

2. Blood volume
   ($p_b \sim v_b = \rho^{\dagger} \cdot V$)

3. Blood Water lifetime
   (τ_b [$k_{po} = \tau_b^{-1}$])

Rooney

7 T

resting-state

22 y female control

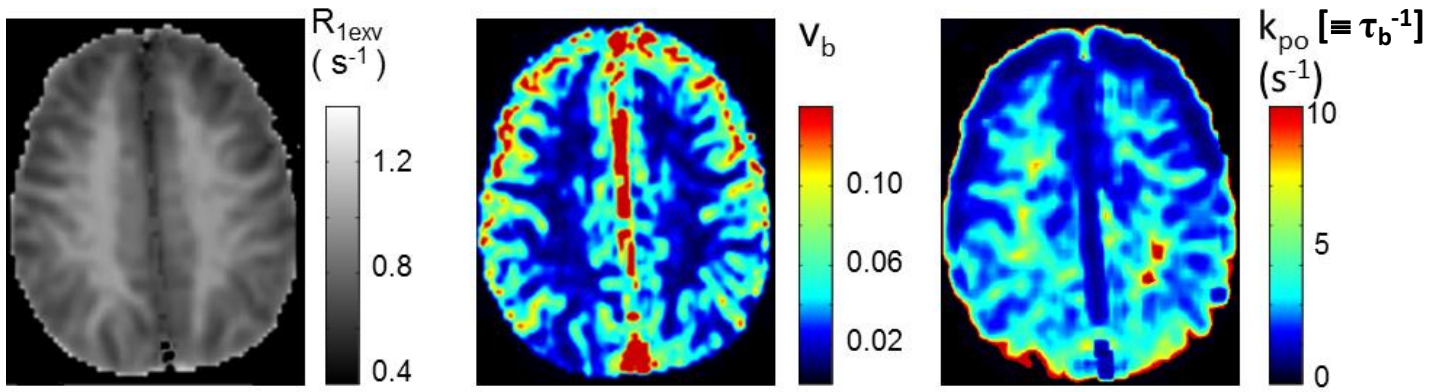

52 y female late-stage MS

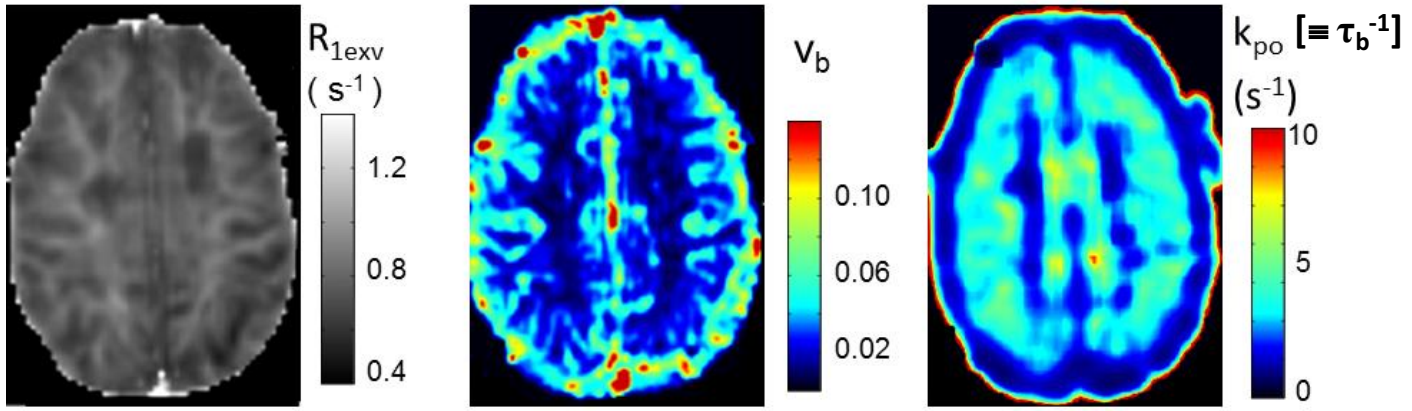

Rooney, Li, Sammi, Bourdette, Neuwelt, Springer (2015)

Table 2. The Biomarker k_{po} Measures Metabolically Activity						
	SSP DCE-MRI (^1H_2O)		^{31}PMRSI	^{23}NaMRSI	SSP DCE-MRI (^1H_2O)	^{31}PMRSI-MT
	v_b	k_{po} $[\tau_b^{-1}]$ (s^{-1})	$[ATP_t]$ (mM)	$[Na_t]$ (mM)	k_{po}·v_b (s^{-1})	CMR_{oxphos} (pmol(ATP)/s/μL)
Healthy Controls (n = 6)						
NWM	0.014	3.2	2.43	19[a]	0.045	50
NGM	0.031	2.9	1.62	31[a]	0.090	160
NGM/NWM					2.0	3.2
Relapsing Remitting MS (n = 6)						
NAWM	0.019	2.2	2.11	27[a]	0.042	
NAGM	0.045	2.0	1.29	36[a]	0.090	
lesion	0.012	1.8		35[a]	0.022	
Glioblastoma (n = 5)						
NA-frontal WM	0.008	2.6		↑3%[b]	0.021	
NA-*thalamus*	0.017	2.9		↓12%[b]	0.049	
NA-*putamen*	0.012	2.5			0.030	
tumor	0.046	≤ 0.18		↑51%[b]	≤ 0.008	
References	this work		78, 79	19, 80	this work	17

[a]reference (19); [b]relative to NWM, reference (80).

17. Zhu, Qiao, Du, Xiong, Liu, Zhang, Ugurbil, Chen (2012).
19. Inglese, Madelin, Oesingmann, Babb, Wu, Stoekel, Herbert, Johnson (2010)
78. Sammi, Berlow, Barbara, Selzer, Grinstead, Kim, Bourdette, Rooney (2012)
79. Sammi, Berlow, Selzer, Maloney, Grinstead, Kim, Bourdette, Rooney, *submitted*
80. Ouwerkerk, Bleich, Gillen, Pomper, Bottomley (2003)

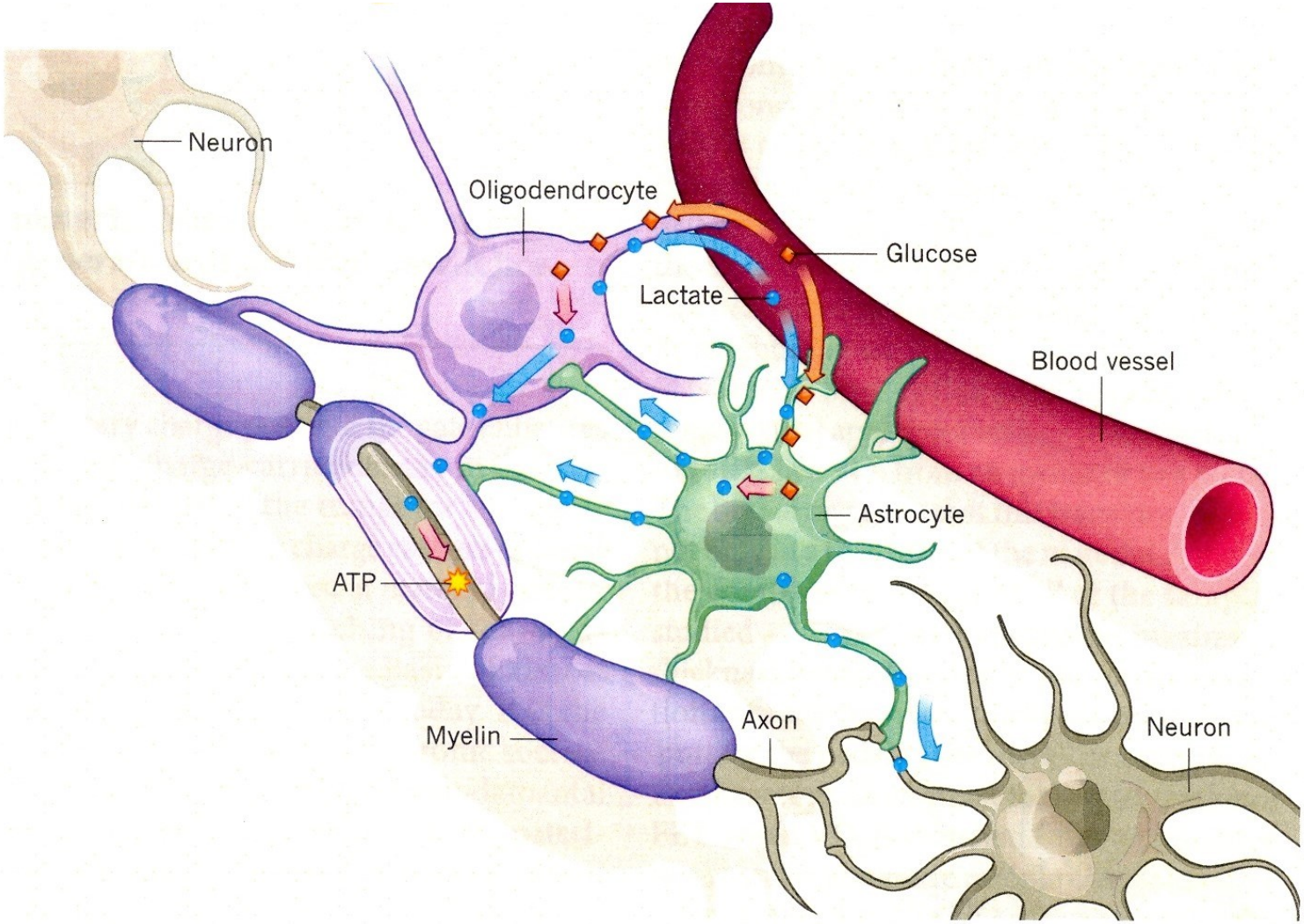

Figure 1 | Metabolic support for neurons. Blood glucose (orange) can be taken up by non-neuronal brain cells known as oligodendrocytes and astrocytes. Inside the cells, glucose is broken down to lactate (blue), which can then be transferred to neurons and used to generate metabolic energy in the form of ATP molecules (yellow). Lee *et al.*[2] show that oligodendrocytes supply nerve fibres (axons) with lactate delivered through a transporter protein (MCT1, not shown) located in the myelin, a membranous sheath around the axons. Lactate can also be produced in astrocytes and then transferred to axons by means of small pores (gap junctions, not shown) through the myelin. In addition, blood lactate may reach neurons through astrocytes and oligodendrocytes.

Rinholm, Bergersen (2012)

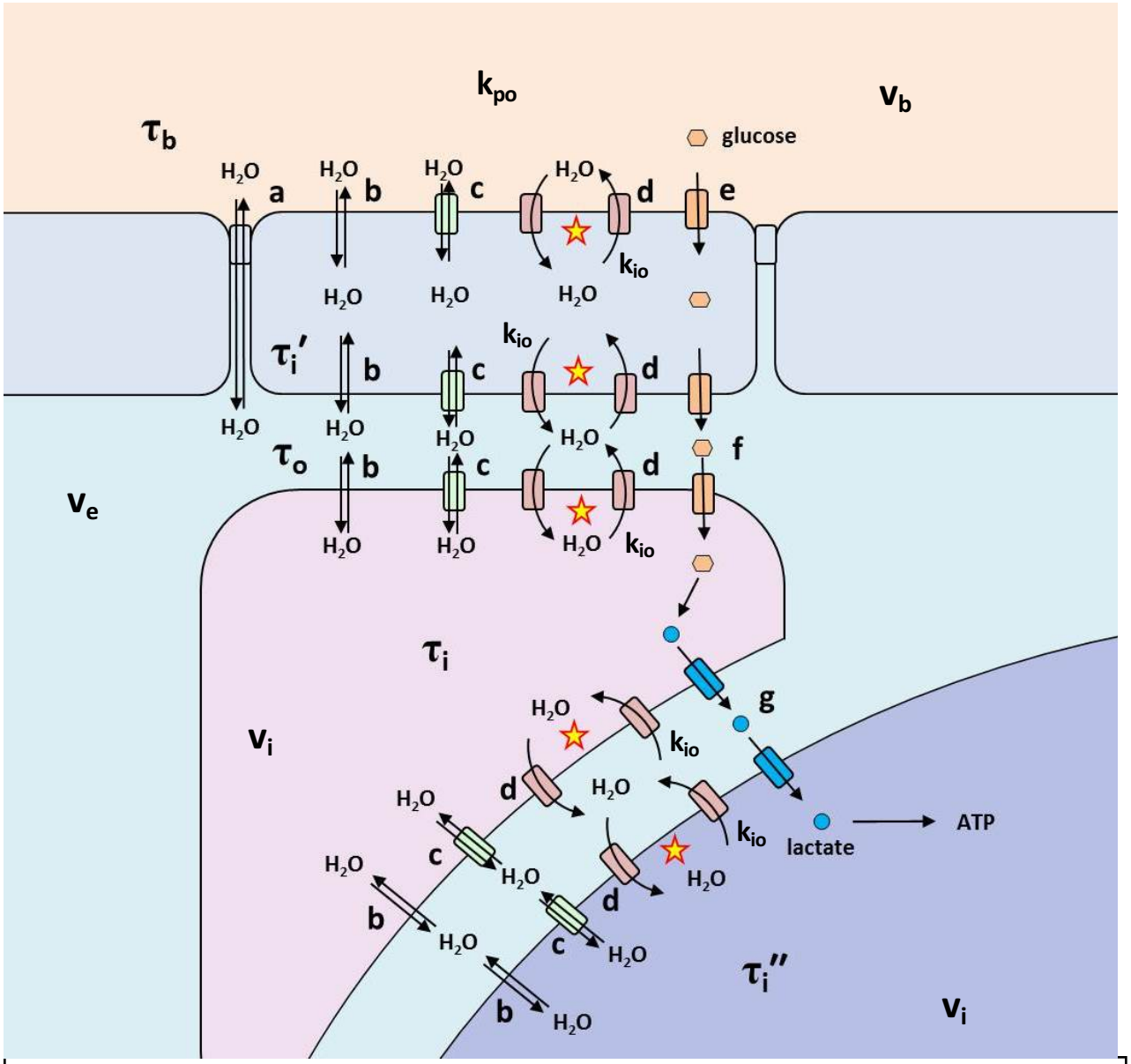

Figure 7. A Neurogliovascular Unit Chain Mechanism. Water exchange processes determine mean water molecule lifetimes in blood (τ_b, beige), interstitium (τ_o, aqua), and endothelial (τ_i', gray), neuroglial (τ_i, pink), and neuronal (τ_i'', blue) cell spaces. The equilibrium paracellular (a), simple diffusion (b), facilitated transcellular (c), and active water cycling (d, stars) pathways are indicated, as are "Magistretti steps" (e,f,g). We suggest the d steps couple unit metabolic activity to τ_b.

Rooney, Li, Sammi, Bourdette, Neuwelt, Springer (2015)

7 T

resting-state

22 y female control

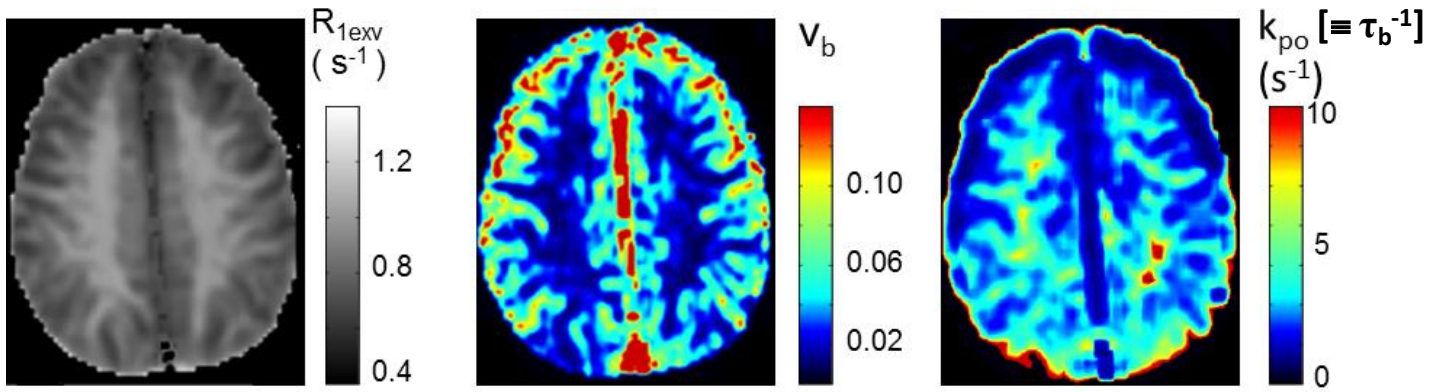

52 y female late-stage MS

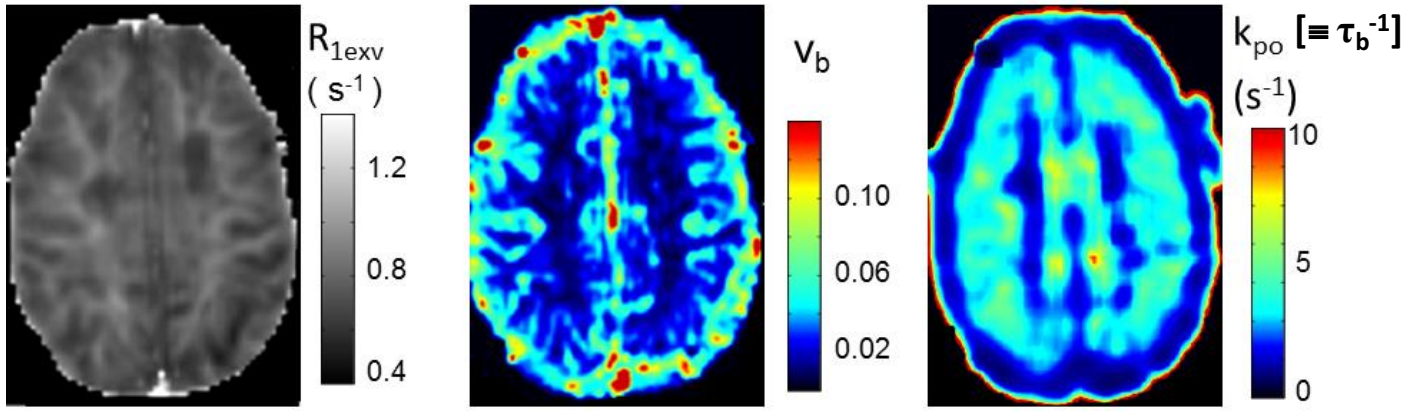

Rooney, Li, Sammi, Bourdette, Neuwelt, Springer (2015)

Metabolic Imaging

- **mapping metabolic thermodynamics**
  - metabolite concentrations [*e.g.*, ^{31}PMRSI]
- **mapping metabolic kinetics**
  - enzyme fluxes [*e.g.*, ^{31}PMRSI-MT]
- **current modalities** [nominal voxel volumes for human study]

  ^{31}PMRSI [$(1.3\ cm)^3 = 2.2\ mL$]; ^{1}HMRSI [$(1\ cm)^3 = 1\ mL$]; SPECT [$(1\ cm)^3 = 1\ mL$];
  HP-^{13}CMRSI [$(7\ mm)^3 = 340\ \mu L$]; PET [$(5\ mm)^3 = 125\ \mu L$]; ^{23}NaMRSI [$(4\ mm)^3 = 64\ \mu L$]
- **potential high-resolution metabolic imaging**

  $^{1}H_2O$ MRI [$(1\ mm)^3 = 1\ \mu L$]

metaboCEST, metaboCESL
- glucoCEST, glucoCESL
- creatiCEST

OHSU
Oregon Health & Science University

Advanced Imaging Research Center

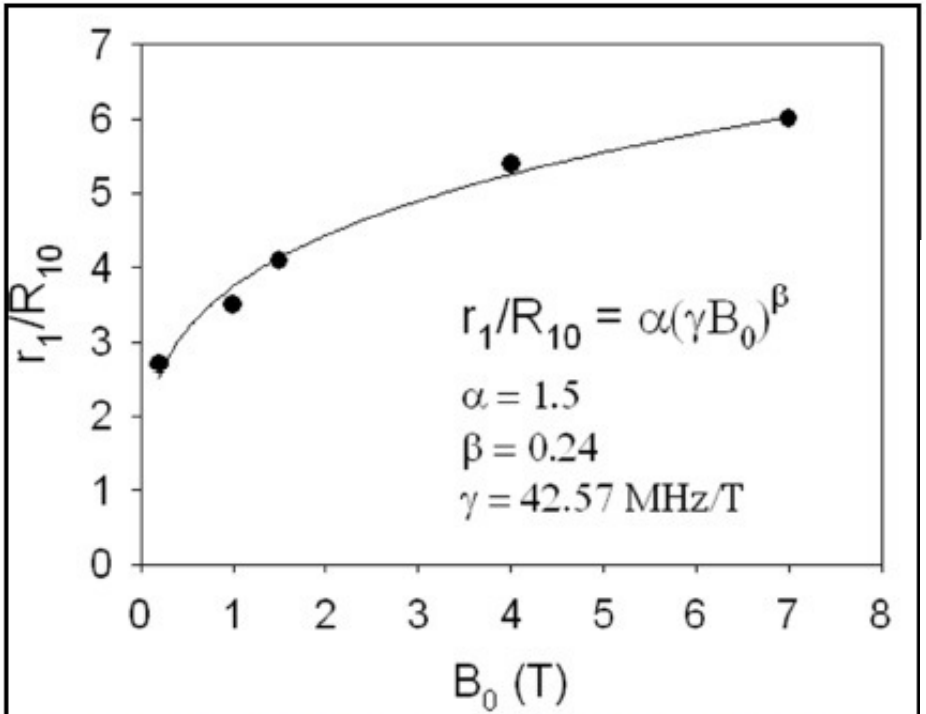

Figure 1. A plot estimating the B_0-dependence of CR detection sensitivity. Filled circles represent the ratio of CR relaxivity to cerebral gray matter ^1H_2O R_1.[1,2] The solid curve represents the power law function with parameters given.

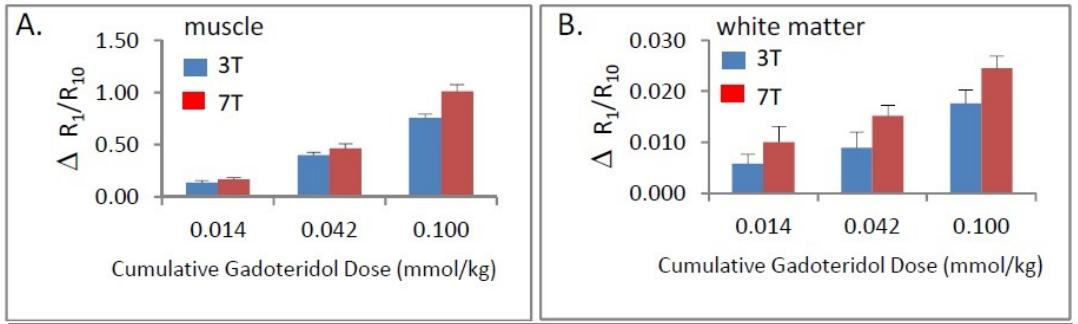

Figure 2. Detection sensitivity of MRI CR in human subjects at 3T and 7T. Subjects were studied using essentially identical MR acquisitions and CR delivery protocols. (**A**) comparison of normalized change in temporalis muscle ^1H_2O R_1 values following three gadoteridol injections (0.014, 0.028, and 0.058 mmol/kg doses; total dose = 0.1 mmol/Kg). For all doses 7T values exceeded those at 3T ($p < 0.001$). The filled bars represent R_1 differences due to B_0 dependence of tissue and CR relaxivities only; contrast to noise differences in base images are not included. (**B**) comparison of normalized change for cerebral white matter ^1H_2O R_1 where CR remains intravascular. Note the much decreased ordinate values in (B) compared to (A). Nevertheless, a significant improvement in CR detectability is realized at 7T compared to 3T ($p < 0.003$).

Rooney, Sammi, Grinstead, Pollaro, Selzer, Li, Springer (2013)

active transmembrane water cycling will alter practice of and/or interpretations of:

- **DCE-MRI**
- **cardiological MRI**
- **fMRI**
- **diffusion-weighted MRI**
- **CEST**
- **magnetization transfer**
- **rotating frame relaxation**
- **MR fingerprinting**

OHSU

Oregon Health & Science University

Advanced Imaging Research Center